Creep–Fatigue Relationship in Polymer: Molecular Dynamics Simulations Approach

Iwan H. Sahputra,* Andreas T. Echtermeyer

The creep-tensile fatigue relationship is investigated using MD simulations for amorphous polyethylene, by stepwise increasing the *R*-ratio from 0.3 for fatigue to an *R*-ratio = 1 for creep. The simulations can produce similar behavior as observed in experiments, for instances strain-softening behavior and hysteresis loops in the stress-strain curves. The simulations predict the molecular mechanisms of creep and fatigue are the same. Fatigue and creep cause significant changes of the van der Waals and dihedral potential energies. These changes are caused by movements of the polymer chains, creating more un-twisted dihedral angles and the unfolding of polymer chains along the loading direction.

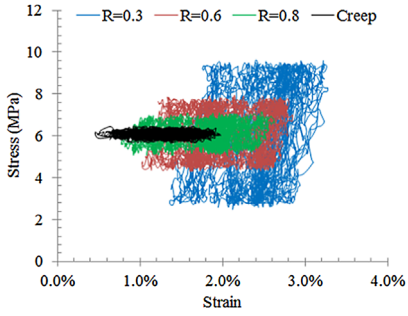

1. Introduction

When polymers are subjected to a constant load, they deform continuously until they break. This behavior, known as creep, has been investigated by many researchers.[1–5] Experimental results are plotted as creep and stress rupture curves. Lifetimes under constant static loads are mainly predicted by fitting the data obtained from the experiments.[3,4]

Polymer components or parts can also be subjected to cyclic or alternating loads known as cyclic fatigue behavior. Fatigue lifetimes are typically obtained by testing and described by S–N curves (stress vs. number of cycles to failure).[6–10] The lifetime of polymers under cyclic loads is also predicted by fracture mechanics using Paris law.[8–10]

Studies of long-term behavior mostly consider creep and fatigue behavior of polymers separately. However, when polymers are subjected to cyclic loading, creep happens simultaneously causing an increase in deformation. In this condition, the time at a certain stress level may be more significant for lifetime calculations than the number of stress cycles.[11,12] Furthermore, components or parts may be subjected to different sequences of constant and cycling loading during service time.

Some work has been performed to investigate the interaction of creep and cyclic fatigue. Bowman and Barker[13] implemented the concept of fractional damage developed previously for the case of metal pressure vessels. Damage is assumed to be introduced into the component from both the fatigue element of loading and from the creep element of loading present in a trapezoidal loading profile. They observed micro-ductility of the fracture surface of a specimen under fatigue testing was similar to that observed under constant load condition. Pinter et al.[14] utilized a linear elastic fracture mechanics (LEFM) approach to model the crack growth in creep and fatigue. They suggested that creep crack growth is a special case of fatigue crack growth. They found the cyclic component of the applied stress dominates crack growth rates at low-test temperature but at high-test temperature the creep component is more dominant. Kadota et al.[15] performed fractographic studies and found the micro-features of creep and fatigue fracture surfaces to be different. However, creep and fatigue showed the same trend of the relation between characteristic size and energy release rate. Based on that, they assumed a similar formation of the process zone under creep and fatigue for crack growth analysis.

Janssen et al.[16] proposed a quantitative fatigue life prediction from a set of creep life data. Their model is based on the hypothesis that the lifetime of polymers under static

I. H. Sahputra, Prof. A. T. Echtermeyer
Engineering Design and Materials Department, Norwegian University of Science and Technology–-NTNU, Trondheim, Norway
E-mail: iwan.h.sahputra@ntnu.no

DOI: 10.1002/mats.201400041

or cyclic loading is only determined by critical strain at which strain softening occurs and the rate of accumulation of plastic strain. They predicted the fatigue lifetime by using a constitutive model, with a defined acceleration factor that indicates how much faster plastic strain is accumulated by cyclic loading compared to its static mean stress. Parsons et al.[17] suggested that the relationship between fatigue and creep can be quantitatively examined by systematically decreasing the dynamic component of fatigue loading. They proposed a power law to describe crack growth rate related to the maximum stress, R-ratio (ratio of minimum to maximum stress in the fatigue test), and temperature. They also proposed an alternative model, a crack growth rate consisting of a creep crack growth rate and a fatigue acceleration factor.

Several empirical models and concepts have been proposed to model this combined behavior. However, creep and fatigue also depend on the internal structure of the polymers that cannot be described by the empirical models. The effects of internal structure are dependent on scale: chemical structure at atomistic level, individual molecular chains, aggregates of chains such as lamellae and spherulites, up to continuum phenomena at the macroscale.[18–21] Models at different length and time scales are needed to describe the phenomena more accurately. Modeling the behavior on all scales is a big task. Here we will limit ourselves to the smallest scale, modeling the creep–fatigue behavior at the atomistic level to provide a better physical basis of the phenomenon.

Molecular dynamics (MD) simulations have been used more and more to study the behavior of polymers on the atomistic scale. Despite of the huge discrepancy between the simulated and laboratory strain rates, some studies have shown that MD is able to predict mechanical properties of polymers deformed at a particular constant rate, such as the Young's modulus, yield stress, and the Poisson's ratio.[22–25] But only a few studies on fatigue behavior of polymers using MD are found, probably because only small samples and short times or a few load cycles can be modeled even with the biggest computers.

Yashiro et al.[26] investigated the effect of loading condition and chain length on the behavior of polyethylene under cyclic loading. Their main finding was the leaf-like hysteresis analogous to experimental results both in stress- and strain-controlled loading, although there was a huge discrepancy in the strain rates. They suggested that short chains might bring the reduction of stiffness and increase of plastic flow deformation. Li et al.[27] studied the thermo-mechanical response of thermosetting polymers, focusing on strain accumulation and energy dissipation. They found that uniaxial stress condition with zero lateral stress lead to the highest rate of strain accumulation compared to purely deviatoric shear stress and uniformly volumetric (hydrostatic) stress. This condition also caused the highest degree of energy dissipation as shown by the highest temperature rising rate calculated by assuming an adiabatic condition.

In this study, the creep–fatigue relationship is investigated using MD simulations under uniaxial stress. Various tensile cyclic fatigue simulations are performed for different R ratios. The relation between creep and fatigue is studied by increasing the R-ratio from 0.3 for tensile cyclic loading to an R-ratio $= 1$ for creep following the similar approach of Parsons et al.[17] The effort shall give some new insight on fundamental physical mechanisms happening inside the material. This is one building block for eventually building a better and more reliable model to predict the creep–fatigue performance of polymers based on fundamental principles.

2. Model, Simulation, and Experiment

2.1. Model and Simulation

The united atom approach, which simplifies each CH_2 monomer of PE as a single atom with molecular weight of 14.02, was used to model the PE. The initial PE chain structure was generated using Monte Carlo self-avoiding random walks similar to the previously developed methods.[28] Each atom was placed on each site of the FCC lattice structure with the lattice constant of 1.53 Å. The model contains ten chains and each chain has 10 000 atoms. The initial atom position was randomly selected and the next atom position was chosen according to the probability for each possible bond angle direction and the density of unoccupied neighbor sites. The functional forms and parameters of the bonded potential[28] and the Lennard–Jones potential parameters of[29] are presented in Table 1. A semi-crystalline model of HDPE is planned to be implemented in the future giving a better representation of the commercial HDPE.

Energy minimizations were performed on the initial structure before running the MD simulations by applying the Polak–Ribiere version of the conjugate gradient algorithm following by Hessian-free truncated Newton algorithm. This was done to speed up the relaxation of high potential energy created during the generation of initial structure. A MD program designed for parallel computers, LAMMPS,[30] was used to equilibrate the initial sample structure and simulate the fatigue process. All the simulations were performed on the supercomputer at NTNU.

Each atom in the model was given an initial velocity by randomly selecting a random number from a uniform distribution at the temperature of 500 K, simulating a molten state. Brownian dynamics simulation of the melted

Table 1. Functional forms and parameters for molecular potential energy.

Interaction	Functional form	Parameters
Bond stretch	$V_b = k_b(r_b - r_o)^2$	$k_b = 350\ \text{kcal mol}^{-1}$ $r_b =$ bond length $r_o =$ equilibrium bond length $= 1.53$ Å
Bond angle bend	$V_a = k_a(\theta_a - \theta_b)^2$	$k_a = 60\ \text{kcal mol}^{-1}$ $\theta_a =$ bond angle $\theta_b =$ equilibrium bond angle $= 109.5^\circ$
Dihedral angle torsion	$V_d = \sum_{n=1}^{4} k_n \cos^{n-1}\phi_d$	$K_1 = 1.73\ \text{kcal mol}^{-1}$, $K_2 = -4.49\ \text{kcal mol}^{-1}$ $K_3 = 0.776\ \text{kcal mol}^{-1}$, $K_4 = 6.99\ \text{kcal mol}^{-1}$ $\phi_d =$ dihedral angle
van der Waals	$V_{ij} = 4\varepsilon_{ij}\left[\left(\frac{\sigma_{ij}}{r_{ij}}\right)^{12} - \left(\frac{\sigma_{ij}}{r_{ij}}\right)^{6}\right],\ r < r_c$	$\varepsilon_{ij} = 0.112\ \text{kcal mol}^{-1}$, $\sigma_{ij} = 4.5$ Å $r_c = 10$ Å

polymer state was performed by applying NVE ensembles and a Langevin thermostat for 10 picoseconds (ps). The Langevin thermostat follows the Langevin equation of motion, where a frictional drag force and a force due to the interaction between solvent and atom are added to the conservative force of each atom due to inter-atom interactions.

The system was then equilibrated at a constant number of particles, pressure, and temperature (NPT) ensembles for 25 ps and then cooled to the temperature of 300 K from 500 K in a stepwise manner within 25 ps simulation time. The final equilibration stage was done for NPT ensembles at the temperature of 300 K for 25 ps. Nose–Hoover thermostat and barostat[31–33] were coupled to the atoms' velocities and simulation box dimensions to control temperature and pressure within NPT ensembles. Time-reversible measure-preserving Verlet and rRESPA integrators[34] were used to integrate the equation of motion. Periodic boundary conditions were applied to all directions of the simulation box so that atoms interact across the boundary.

The model of the polymer had a characteristic ratio (C_N) of 7.34 at 500 K (=227 °C) and C_N is defined as:

$$C = < r^2 > / nl^2 \quad (1)$$

where $<r^2>$ is the average end-to-end distance of the chain, n is the number of chains, and l is bond length. By direct intrinsic viscosity measurement,[35] C_N of PE was found to be 7.10, 6.99, and 6.80 at temperatures of 127.5, 142.2, and 163.9 °C, respectively. Characteristic ratios (C_N) from 8.7 to 10.5 were found by light scattering measurement[36] on linear PE in diphenyl at 400 K (=127 °C). Therefore the model has a C_N value in the range of the laboratory measurements and indicates it has reached the unperturbed state. Figure 1 shows the structural geometries of the model at the temperature of 300 K.

Figure 2 shows the specific volume of the model as a function of temperature after the final equilibration stage. Temperature was gradually increased from 300 to 500 K within 50 ps of a NPT ensembles simulation. It can be seen that the model does not show crystallization behavior as typically observed in laboratory measurement data for a high crystallinity PE sample.[37] The specific volume of a high crystallinity PE sample will increase rapidly as the temperature approaches the melting temperature. A low crystallinity PE sample, like this model, shows a gradual increase of the specific volume with temperature.

Tensile fatigue was simulated by imposing a sinusoidal stress in one longitudinal direction during a dynamic run. The fatigue stress was produced by updating pressure of the sample sinusoidally in a stepwise manner in one longitudinal direction. Various R-ratios (0.3, 0.6, and 0.8) with a mean stress of 6 MPa were applied as shown in Figure 3. The loading conditions will deform the sample with a strain rate in order of 10^8–10^{10}/s depending on the slope of the sinusoidal load and R-ratio. This strain rate is several orders higher than in typical laboratory experiments; however, the general conclusions from the simulations would contribute in further understanding of fatigue–creep relationships of amorphous PE. Creep was simulated by applying a constant stress in one longitudinal direction. For both fatigue and creep simulations, the other two transverse directions of the simulation box were kept at zero applied stress, allowing the box to contract sideways.

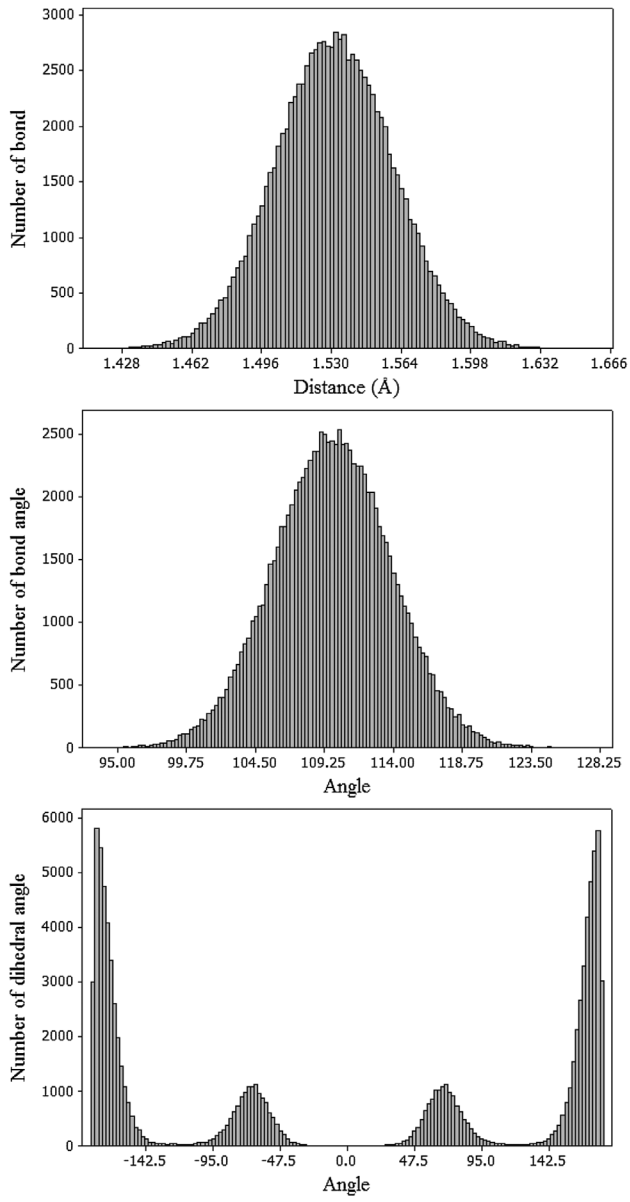

Figure 1. Polymer chain configurations after equilibrium process at the temperature of 300 K.

Tensile strain is unit-less and is defined as the length change divided by the original box length.

2.2. Experiment

A few simple exploratory stress controlled tensile fatigue and creep experiments were also performed in the laboratory at room temperature for comparing quantitatively the predictions of the simulation results. A sinusoidal displacement was applied at a frequency of 2 Hz, mean stress of 6 MPa, and *R*-ratios of 0.3, 0.6, and 0.8. Creep tests were also performed applying a

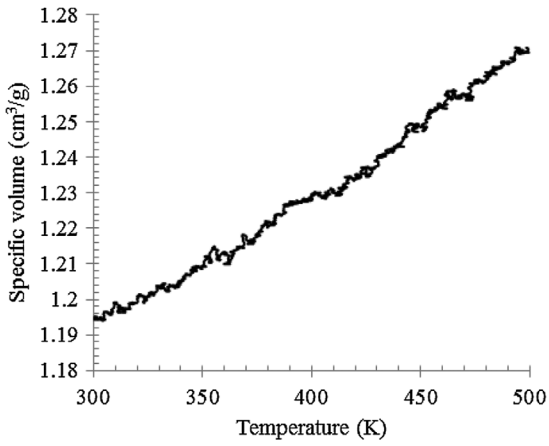

Figure 2. Specific volume versus temperature.

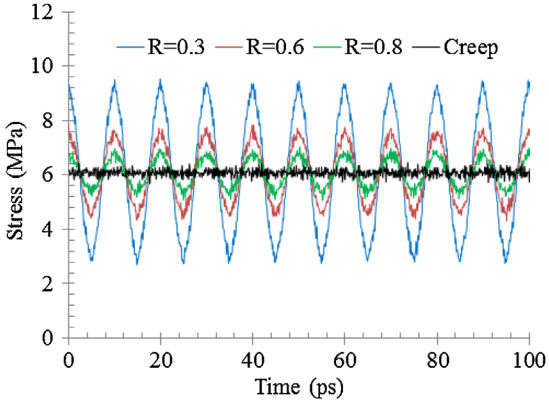

Figure 3. Cyclic loading for various *R*-ratios and creep in the MD simulations.

constant stress of 6 MPa. The test samples were cut from a PE sheet "Polystone M-Black-AST" manufactured by Rochling Engineering Plastic. It is a high-density polyethylene (HDPE), which has a molecular weight of 9.2×10^6 g mol^{-1} and a density of 0.945 g cm^{-3}. The comparison with HDPE is not ideal; however, the experiments were performed to show general trends of fatigue and creep behavior.

The shape and dimension of the samples were according to ISO 527-2:2012 type 1B standard and the thickness was 3 mm. Loads were recorded by a computerized data acquisition system. Stresses were calculated as load of initial cross sectional area (engineering stresses). The initial measurements from 0 to 10 s were not used because the test machine had not reached the steady state stress amplitude yet. At least two experiments were performed per test condition for obtaining the principle characteristics of HDPE. More repeated testing would be needed to obtain proper material parameters, but considering the general

discrepancies between model and experiment, this approach was seen as being sufficient.

3. Results and Discussion

3.1. Mean Strain-Cycle and Stress–Strain Behavior

Figure 4 presents the strain responses to the fatigue loading with different *R*-ratios and creep, calculated by MD. The mean strain was calculated by averaging the strain in one cycle of loading. Creep has no loading cycle, however, for the purpose of comparison the mean strain was calculated also by averaging the strain in a period of time corresponding to one loading cycle. There are fluctuations in the mean strain response although the sinusoidal loading stress is smooth as shown in Figure 3. Stress was controlled using a Berendsen barostat[38] in the MD simulations by coupling the system to a constant pressure bath. Berendsen barostat accomplishes this by rescaling the system volume and proportionally rescaling all atoms to new positions within the simulation box every time-step. Coupling to a constant pressure bath introduces volume (density) fluctuations thus causing fluctuations in the length of simulation box.[38] These fluctuations are then reflected in the strain fluctuations of Figure 4.

For the simulations, the mean strain increases along with the number of cycles in all the fatigue and creep calculations indicating a strain-softening behavior. The lowest *R*-ratio (=0.3) fatigue produces the highest mean strain. In the stress–strain curves, the hysteresis loop areas are small indicating little energy spent in the cycle and therefore small temperature changes.

Laboratory mean strain-number of cycle curves and stress–strain curves of the various *R*-ratios fatigue and creep experiments are presented in Figure 5. As predicted by the simulations, the mean strain increases along with the cycle for all experiments while the lowest *R*-ratio (=0.3) fatigue produces the highest mean strain. The experiments of this study show higher strain increases during creep than cyclic fatigue, while the absolute strains were again higher for fatigue. Other experimental studies found that the strain increase increases with the combination of creep and fatigue,[16] but these studies were done for longer times and

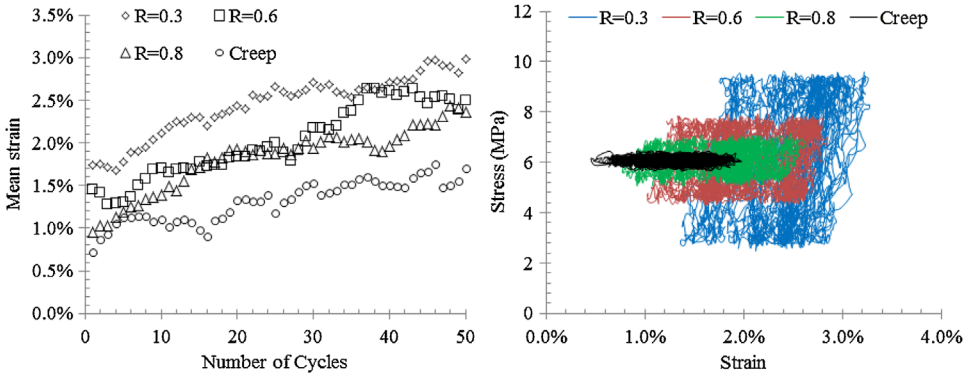

Figure 4. Mean strain versus number of cycles and stress–strain curves for cyclic loading at different *R*-ratios and creep from the MD simulations.

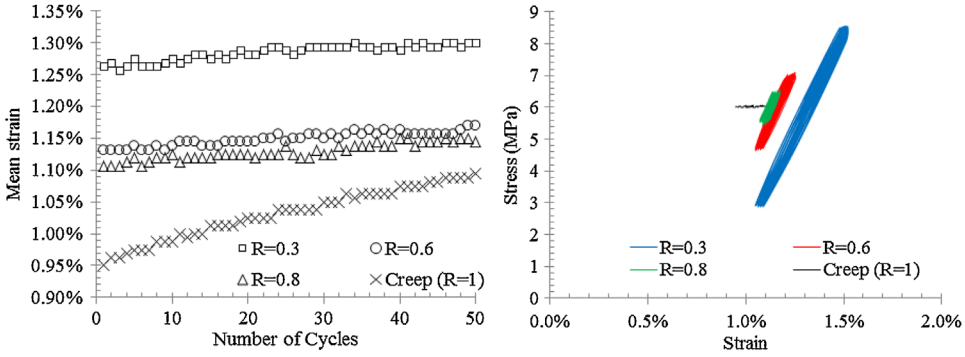

Figure 5. Mean strain versus number of cycles and stress–strain curves for cyclic loading at different *R*-ratios and creep from the experiments.

larger number of cycles. The experiments here were just done for short times for comparison with the MD simulations.

The MD simulations are able to reproduce similar trends as the experiments although there are discrepancies in the quantities. The MD simulations could show the effect of creep and accelerated creep due to additional cyclic loading. This is consistent with the experiments reported here and previous experimental work.[16] There is not enough data to calculate the time-to-failure using an acceleration factor, as was done in.[16] However, the simulations indicate that the increase in strain with number of cycles is fairly constant regardless of the *R*-ratio. But the absolute strain is determined in the first cycle due to the *R*-ratio.

Another way to look at the effects of fatigue is to investigate the fatigue modulus. The fatigue modulus is defined as the slope of the stress–strain curve in each cycle, corresponding to the secant modulus in monotonic loading. Table 2 presents the fatigue modulus of the simulations and experiments. The stress (or strain) rate effect has a big impact on the stiffness at the first cycle in the MD simulations as indicated by the increasing of fatigue modulus along the decreasing of *R*-ratio. The higher *R*-ratio, the smaller the stress amplitude (at the same mean stress). Therefore, the high *R*-ratio has a slower stress rate. The stress rate (or strain rate) effect on the fatigue modulus is almost negligible for the experiments, because the experimental frequency is much smaller and varies less than in the MD simulations. After 50 cycles, the changes of the fatigue modulus are not significant both in the MD simulations and experiments.

The discrepancy in fatigue modulus between simulations and experiments, in addition to the stress (or strain) rate effect, is influenced by the differences in morphology. Runt and Jacq[39] showed an effect of the degree of crystallinity on the fatigue crack propagation in PE, the increasing of crystallinity improves fatigue resistance. Sharif et al.[40] found an increase in storage modulus with degree of crystallinity. Boiko et al.[41] presented the increasing of dynamic storage modulus with the draw ratio. In this study the simulation model is amorphous PE while the experimental samples are HDPE with a high degree of crystallinity. Therefore, it is expected to see a lower fatigue modulus for the amorphous material. However, it is interesting that the amorphous PE model is able to predict hysteresis loops in the stress–strain curves as typically observed in HDPE under fatigue loading.[42,43] The simulation also shows a significant increase of modulus with decreasing *R* ratio (increasing stress rate). This expected increase is typical for amorphous materials but less so for crystalline materials. The experiments of the semi crystalline HDPE showed only a very small or no increase in modulus.

3.2. Potential Energy and Structural Geometry Development

MD simulations give the opportunity to investigate potential energy changes and microstructure changes due to creep and fatigue. Creep reduces the mean potential energy slightly more than fatigue, as shown in Figure 6. The van der Waals and dihedral energies contribute most to the change of potential energy. They are reduced by about 1 600 and 700 kcal mole^{-1}, respectively at the end of the MD simulations. Bond and angle energies change only slightly, because they are stronger bonding energies compared to the van der Waals and dihedral energies.

Combining the observations of increased strain with number of cycles and creep with the energy changes, the strain increases are related to changes in van der Waals and dihedral energies. This indicates that the polymer chains slide against each other and rotate themselves into an alignment with the direction of the applied stress. This behavior is as expected for polymers, but it shows that MD can predict this behavior from fundamental principles.

Interactions between non-bonded atoms are represented by the van der Waals energy. In a polymer system these interactions are between atoms or molecules on the different chains. Therefore the van der Waals energy governs the resistance of polymer chains for sliding against each other when cyclic loading is applied. Increasing the well depth (ε_{ij}) parameter of the van der Waals energy function will increase the resistance. Short time simulations of fatigue with $R = 0.3$ using an arbitrary higher ε_{ij} parameter were performed. The ε_{ij} parameter was set to be 10% higher (=0.123 kcal mol^{-1}) than the original simulations and the results were compared to the original simulations. Figure 7 shows that the simulations using a higher van der Waals parameter produce lower mean

Table 2. R-ratio effect on fatigue modulus (MPa) of the MD simulations and experiments.

	MD simulations			Experiments		
Cycle	$R = 0.8$	$R = 0.6$	$R = 0.3$	$R = 0.8$	$R = 0.6$	$R = 0.3$
1	346	730	1 352	1 292	1 318	1 283
50	295	757	1 252	1 322	1 411	1 264

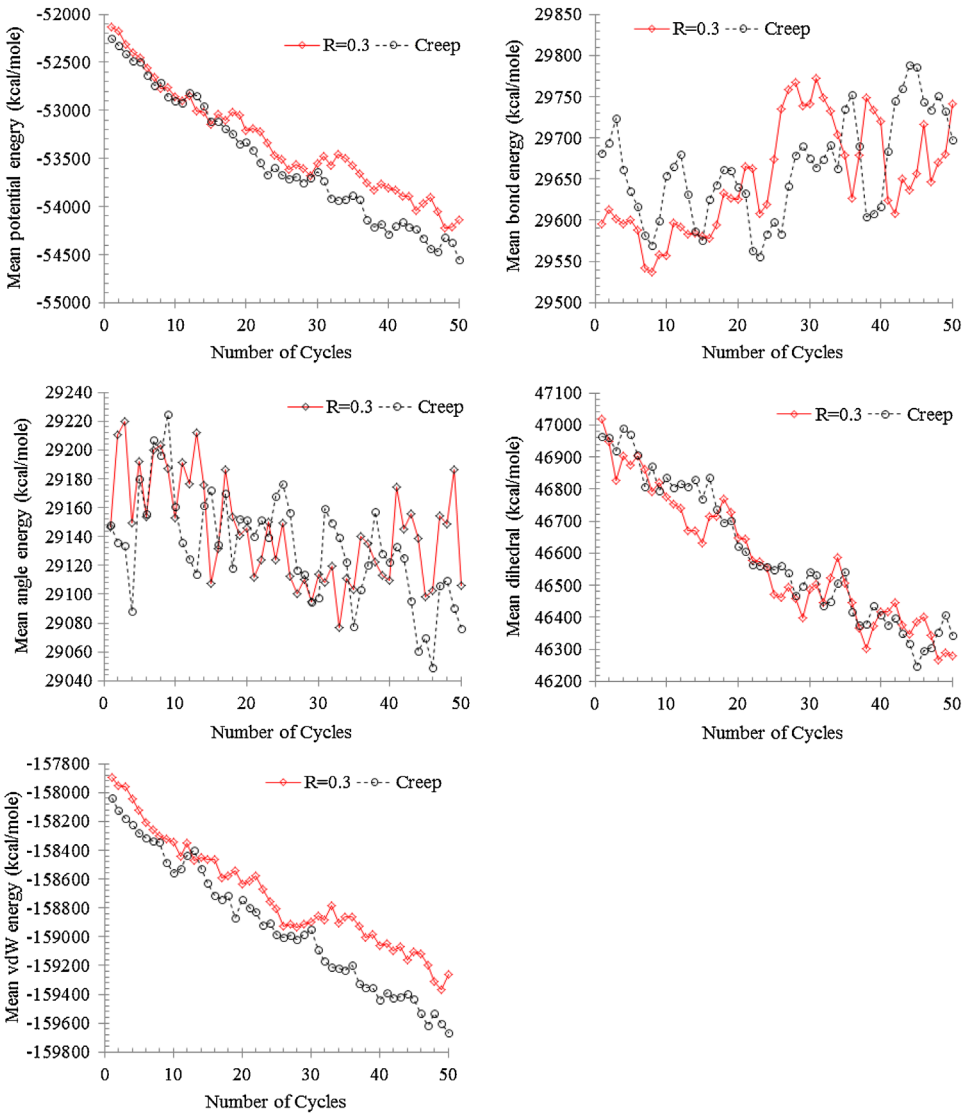

Figure 6. Development of mean energy with increasing number of cycles/time for fatigue ($R = 0.3$) and creep in the MD simulations.

strain, indicating higher resistance to the sliding movement of the polymer chains. In addition the mean strain does not seem to increase with the number of cycles, indicating that creep is reduced. However, more simulations will have to be made to explore these effects further.

MD calculations also allow a direct simulation of the geometrical changes of a polymer. Table 3 presents the changes of structural configurations of the polymer chains at the equilibrium (initial) before any loading and at the end of the simulations. Significant change can only be seen in the percentage of the dihedral angles in the Trans state before and after loading. The percentage increases by about 2%. This change is consistent with the changes in the van der Waals and dihedral potentials. The bond distances and angles do not show any significant changes. It should be noted that the simulations were performed for only 50 cycles due to limited computer power, but as long as polymer chain movements do not get very large, the trends shown here should remain the same also for larger number of cycles.

Table 4 shows the average radius of gyration of all chains before any loading and after 50 cycles of the fatigue loading. This property is an indication of the level of compaction or how folded or unfolded the chains are. The radius of gyration of a chain was calculated following Equation 2:

$$R_g^2 = \frac{1}{M}\sum m_i(r_i - r_{cm})^2 \quad (2)$$

where M is the total mass of the chain, r_{cm} is the center-of-mass position of the chain.[44] The x, y, and z components of the radius of gyration tensor can be determined using the same formula.

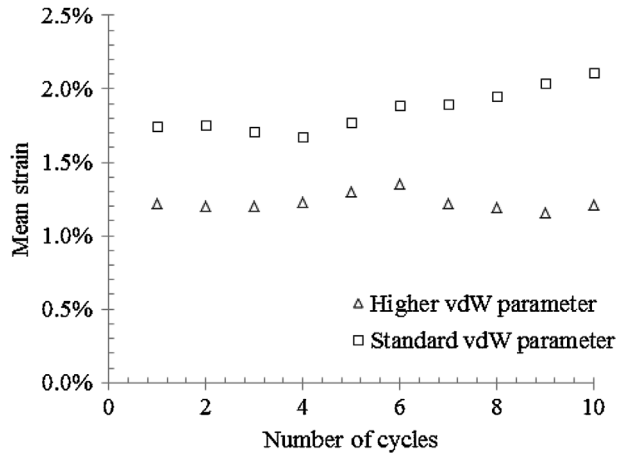

Figure 7. Effect of low and high van der Waals (vdW) parameters on the mean strain in the fatigue simulations with $R = 0.3$.

It can be seen in Table 4 that the average of the radius of gyration about the x-axis (the loading direction) increases with the number of cycles, while the other two directions (y and z) decrease. The chains tend to align along the loading direction. A low R-ratio (=0.3) of fatigue loading tends to increase the average of radius of gyration more than a high R-ratio and creep. This also indicates that the mean strain is related to the radius of gyration.

Table 4. Average of the radius of gyration (R_g) before and after loading.

	Average R_g (Å)		
	x	***y***	***z***
Initial	1 680	1 813	1 812
After loading:			
Creep	1 731	1 758	1 758
$R = 0.8$	1 755	1 765	1 744
$R = 0.6$	1 762	1 746	1 751
$R = 0.3$	1 781	1 743	1 734

From the calculations of potential energies and structural geometry development, MD did not show any changes in deformation mechanisms between creep and tensile fatigue. This confirms previous experimental work[13,15] that indicated the same processes are happening in both conditions. If fatigue and creep are based on chains sliding against each other as indicated by the MD simulations, it can be speculated that blocking the possibility to slide would increase fatigue and creep performance. In the case of amorphous PE this seems to happen when the molecules move and align themselves, they eventually crystallize.

Table 3. Chain geometries at the end of the simulations.

		Fatigue with R-ratio			
	Creep ($R = 1$)	**0.8**	**0.6**	**0.3**	**Initial**
Bond distance					
Mean	1.53	1.53	1.53	1.53	1.53
Std. Dev.	0.03	0.03	0.03	0.03	0.03
Bond Angle					
Mean	109.70	109.70	109.70	109.71	109.75
Std. Dev.	3.97	3.99	3.97	3.98	4.03
Dihedral angle: Trans state					
Mean	170.07	170.06	170.11	170.08	169.74
Std. Dev.	8.12	8.15	8.11	8.17	8.48
Pct. (%)	74.86	74.97	74.97	74.93	72.84
Dihedral angle: Gauche (+) state					
Mean	68.24	67.97	68.42	68.38	68.78
Std. Dev.	13.03	13.09	13.22	12.98	13.64
Pct. (%)	12.54	12.47	12.61	12.48	13.52
Dihedral angle: Gauche (−) state					
Mean	−68.22	−68.12	−68.30	−68.35	−68.61
Std. Dev.	13.09	13.13	12.99	13.12	13.67
Pct. (%)	12.60	12.56	12.42	12.59	13.64

This causes stiffening and improved fatigue performance, closer to the performance of highly crystalline PE fibers. With today's computer power MD cannot model this entire process, but probably in a couple of years computers will be powerful enough to make this possible. MD should also be able to simulate how easily different types of polymer chains can move against each other. This could be used to predict creep and tensile fatigue performance of various kinds of polymers.

4. Conclusions

Creep–fatigue relationships were investigated by MD simulations on the molecular and global level. Stress controlled conditions were modeled using a Berendsen barostat.

The relation between creep and fatigue was studied by simulating loading at various R-ratios ($R = 0.3$, 0.6, and 0.8) for tensile cyclic fatigue and an $R = 1$ for creep. The MD simulations are able to produce qualitatively similar behavior as observed experimentally in the laboratory, for instances strain-softening behavior and hysteresis loops in the stress–strain curves. Increasing R-ratio reduces mean strain and creep produces the lowest mean strain. These trends were properly reproduced even though simulations were done at much higher stress (or strain) rates and used an amorphous polyethylene model.

For the simple amorphous PE modeled here, MD could predict that cyclic fatigue increases strain growth with number of cycles (or time) compared to simple creep. The movements of the polymer chains are due to creating more un-twisted dihedral angles. The polymer chains unfold along the loading direction. Bond angles and distances change only slightly, demonstrated by small changes in bond and angle potentials. This was shown by simulations of the radius of gyrations and an evaluation of the potential energies of the system. Preliminary calculations showed that a simulated increase in van der Waals forces reduces the effects of fatigue and creep.

Acknowledgements: This research was financed by the Norwegian University of Science and Technology (NTNU). Computational resources at NTNU were partially provided by NOTUR, http://www.notur.no. This support is gratefully acknowledged.

Received: May 5, 2014; Revised: August 30, 2014; Published online: November 3, 2014; DOI: 10.1002/mats.201400041

Keywords: creep; fatigue; molecular dynamics; polyethylene

[1] H. B. H. Hamouda, M. Simoes-betbeder, F. Grillon, P. Blouet, N. Billon, R. Piques, *Polymer* **2001**, *42*, 12.
[2] A. D. Drozdov, Q. Yuan, *Int. J. Solids Struct.* **2003**, *40*, 10.
[3] R. K. Krishnaswamy, *Polymer* **2005**, *46*, 25.
[4] R. Khelif, A. Chateauneuf, K. Chaoui, *Int. J. Press. Vessels and Pip.* **2007**, *84*, 12.
[5] K-h. Nitta, H. Maeda, *Polym. Test.* **2010**, *29*, 1.
[6] R. Khelif, A. Chateauneuf, K. Chaoui, *Meccanica* **2008**, *43*, 6.
[7] A. J. Lesser, *J. Appl. Polym. Sci.* **1995**, *58*, 5.
[8] M. G. Wyzgoski, G. E. Novak, *J. Mater. Sci.* **2005**, *40*, 2.
[9] G. Pitman, I. M. Ward, *J. Mater. Sci.* **1980**, *15*, 3.
[10] M. Wyzgoski, G. Novak, *J. Mater. Sci.* **2008**, *43*, 8.
[11] J. Roesler, H. Harders, M. Baeker, *Mechanical Behaviour of Engineering Materials*, Springer, Berlin, Heidelberg **2007**.
[12] D. R. Moore, J. G. Williams, A. Pavan, *Fracture Mechanics Testing Methods for Polymers, Adhesives and Composites*, Elsevier, **2001**.
[13] J. Bowman, M. B. Barker, *Polym. Eng. Sci.* **1986**, *26*, 22.
[14] G. Pinter, W. Balika, R. W. Lang, *European Structural Integrity Society*, Elsevier, **2002**.
[15] K. Kadota, S. Chum, A. Chudnovsky, *J. Appl. Polym. Sci.* **1993**, *49*, 5.
[16] R. P. M. Janssen, L. E. Govaert, H. E. H. Meijer, *Macromolecules* **2008**, *41*, 7.
[17] M. Parsons, E. V. Stepanov, A. Hiltner, E. Baer, *J. Mater. Sci.* **2000**, *35*, 11.
[18] J. Crawshaw, A. H. Windle, *Fibre Diffract. Rev.* **2003**, *11*, 52.
[19] K. Kremer, F. Müller-Plathe, *Mol. Simulat.* **2002**, *28*, 8.
[20] S. A. Baeurle, T. Usami, A. A. Gusev, *Polymer* **2006**, *47*, 26.
[21] J. Baschnagel, K. Binder, P. Doruker, A. Gusev, O. Hahn, K. Kremer, W. Mattice, F. Müller-Plathe, M. Murat, W. Paul, S. Santos, U. Suter, V. Tries, *Viscoelasticity, Atomistic Models, Statistical Chemistry*, Springer, Berlin/Heidelberg **2000**.
[22] D. Brown, J. H. R. Clarke, *Macromolecules* **1991**, *24*, 8.
[23] L. Yang, D. J. Srolovitz, A. F. Yee, *J. Chem. Phys.* **1997**, *107*, 11.
[24] F. M. Capaldi, M. C. Boyce, G. C. Rutledge, *Polymer* **2004**, *45*, 4.
[25] I. H. Sahputra, A. T. Echtermeyer, *Model. Simulat. Mater. Sci. Eng.* **2013**, *21*, 065016.
[26] K. Yashiro, M. Naito, S. Ueno, F. Jie, *Int. J. Mech. Sci.* **2010**, *52*, 2.
[27] C. Li, E. Jaramillo, A. Strachan, *Polymer* **2013**, *54*, 2.
[28] D. Hossain, M. A. Tschopp, D. K. Ward, J. L. Bouvard, P. Wang, M. F. Horstemeyer, *Polymer* **2010**, *51*, 25.
[29] W. Paul, D. Y. Yoon, G. D. Smith, *J. Chem. Phys.* **1995**, *103*, 4.
[30] S. Plimpton, *J. Comput. Phys.* **1995**, *117*, 1.
[31] W. Shinoda, M. Shiga, M. Mikami, *Phys. Rev. B* **2004**, *69*, 13.
[32] G. J. Martyna, D. J. Tobias, M. L. Klein, *J. Chem. Phys.* **1994**, *101*, 5.
[33] M. Parrinello, A. Rahman, *J. Appl. Phys.* **1981**, *52*, 12.
[34] E. T. Mark, A. José, L.-R. Roberto, L. J. Andrea, J. M. Glenn, *J. Phys. A: Math. Gen.* **2006**, *39*, 19.
[35] A. Nakajima, F. Hamada, S. Hayashi, *J. Polym. Sci. Part C: Polym. Symp.* **1967**, *15*, 1.
[36] Y. Muraoka, K. Kamide, H. Suzuki, *Br. Polym. J.* **1983**, *15*, 2.
[37] S. Matsuoka, *J. Polym. Sci.* **1962**, *57*, 165.
[38] H. J. C. Berendsen, J. P. M. Postma, W. F. van Gunsteren, A. DiNola, J. R. Haak, *J. Chem. Phys.* **1984**, *81*, 8.
[39] J. Runt, M. Jacq, *J. Mater. Sci.* **1989**, *24*, 4.
[40] A. Sharif, N. Mohammadi, S. R. Ghaffarian, *J. Appl. Polym. Sci.* **2009**, *112*, 6.
[41] Y. M. Boiko, W. Brostow, A. Y. Goldman, A. C. Ramamurthy, *Polymer* **1995**, *36*, 7.
[42] K. Hizoum, Y. Remond, S. Patlazan, *J. Eng. Mater. Technol.* **2011**, *133*, 3.
[43] S. T. T. Nguyen, S. Castagnet, J.-C. Grandidier, *Int. J. Fatigue* **2013**, *55*, 166.
[44] U. W. Gedde, *Polymer Physics*, Chapman & Hall, **1995**.